An improved CA-CFAR method for ship target detection in strong clutter using UHF radar

Article *in* Signal Processing Letters, IEEE · August 2020

DOI: 10.1109/LSP.2020.3015682

An improved CA-CFAR method for ship target detection in strong clutter using UHF radar

Chunming Kuang, Caijun Wang, Biyang Wen, Yidong Hou, and Yeping Lai

***Abstract*—In this paper, the application of ultra-high frequency (UHF) radar for ship target detection over river is investigated for the first time. Due to the wide beam width of antenna, the ship detection of the UHF radar suffers from the broaden river clutters scattering from water waves. In addition, due to the high resolution, the ship echoes are seriously extended in both range and Doppler dimensions, which is different from the traditional point target signal. Extended target detection in strong river clutter is applied in this paper. Conventional constant false alarm rate (CFAR) detector is limited in this situation, which is applicable to the point target detection in clutter free background. An improved cell-averaging (CA)-CFAR method is proposed based on a joint estimation of threshold in range, Doppler and time serials of range-Doppler (R-D) spectra. Based on the time stationarity of clutter, this three-dimensional (3D) CA-CFAR combines several R-D spectra collected in continuous time to estimate the clutter threshold. The effectiveness of this improved method is validated using both simulated and field data.**

***Index Terms*—extended target, improved CA-CFAR method, R-D spectrum, strong clutter, target detection, UHF radar**

I. Introduction

Target detection is a key problem in radar technology. At present, the commonly used detectors are constant false alarm rate (CFAR) detector [1] [2], or adaptive detector possessing CFAR property [3]. There are two common CFAR detectors. One places the reference units in the surrounding area of detection unit in space to estimate clutter, called airspace-CFAR method. The representative methods are cell-averaging (CA) [4] [5] and order statistics (OS) [6]. Another kind scans the detection unit many times to estimate clutter, called time sequence CFAR method, also known as clutter-map method [7]. Conventional CFAR uses a straightforward thresholding detection in the spectral domain, either range or Doppler space [8] [9]. The peak point (i.e., point target) with the SCR (signal to clutter ratio) above a preset threshold is identified in a single sample of the range-Doppler (R-D) spectrum. Sequential multi-stage detection performed both in range dimension and Doppler dimension is also available [10]. Kronauge and Rohling proposed a two-dimensional (2D) CFAR based on a combination of OS and CA CFAR [11] [12]. Zhang and Li proposed a 2D CA-CFAR in R-D spectrum [13]. Dzvonkovskaya *et al*. applied a three-dimensional (3D) OS-CFAR in range, Doppler and azimuth beam direction [14] [15] [16].

Ultra-high frequency (UHF) radar has been used for river surface velocity [17] and discharge measurement [18]. Meanwhile, it can detect and track ship targets moving on the water [19]. Due to the wide beam width of antenna, the ship detection of the UHF radar suffers from the broaden river clutters scattering from water waves [20]. In addition, due to the high resolution, the ship echoes are seriously extended in both range and Doppler dimensions. However, conventional CFAR methods are generally applicable to the point target detection. In view of this, an improved CA-CFAR method is proposed for the UHF radar to detect the extended target in strong river clutter, which is a 3D CA-CFAR detector in range, Doppler and time serials of R-D spectra. A range-Doppler-time 3D joint estimation of threshold is introduced to the CA-CFAR detector, in which the adjacent R-D spectra are involved to estimate the detection threshold.

This paper is structured as follows: Firstly, we focus on the characteristic analyses of the ship target signal and clutter in the R-D spectrum. Secondly we introduce the improved CA-CFAR method. Then we demonstrate the validity of the proposed method by detecting simulated targets as well as real targets with experimental data. At last we make conclusions.

II. Characteristics analysis in R-D spectrum

The linear frequency modulated interrupted continuous wave (FMICW) is chosen for the waveform of the UHF radar, which operates at a center frequency of 334 MHz, a bandwidth of 10 MHz, and a sweep period of 41 ms. The maximum detection

TABLE I
UHF radar Parameters

Parameters	Numerical Value
carrier frequency	334 MHz
bandwidth	10 MHz
transmitting power	250 mW
frequency-sweeping period	41 ms
antenna gain	7.5 dBi
antenna beam width	90 Deg
range resolution	15 m
maximum unambiguous velocity	5.5 m/s
maximum unambiguous range	500 m

This work was supported in part by the National Natural Science Foundation of China under Grant 41706200 and 61671331, and by the National Key R&D Program of China under Grant 2017YFC0405703.

Chunming Kuang, Biyang Wen, Caijun Wang, Yidong Hou and Yeping Lai are with the Radar and Signal Processing Laboratory (RSPL), Electronic Information School, Wuhan University, Wuhan 430072, China (Corresponding author: Caijun Wang (wcj@whu.edu.cn); Biyang Wen (bywen@whu.edu.cn))

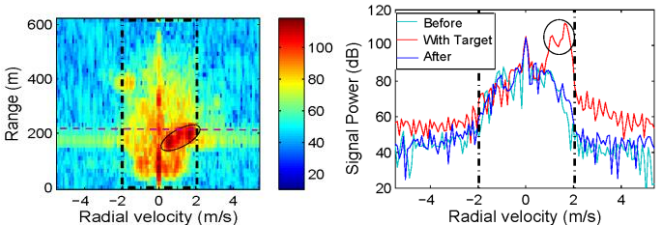

Fig. 1. Echo Spectrum of UHF radar. (a) R-D spectrum. (b) Doppler spectrum of the 15th range bin.

range is designed to be 500 m for a transmitting power of 250 mW, with a range resolution of 15 m. The maximum detection velocity is 5.5 m/s, with a velocity resolution of 0.086 m/s. A 5-element Yagi antenna is vertically polarized for transmitting signal, with a directional gain of 7.5 dBi and wide beam width of 90 °. Three other identical Yagi antennas are deployed in a linear array for the receiving antenna. Table I shows the radar parameters [17].

Fig. 1(a) shows a typical R-D spectrum of the UHF radar, observed on the bank of Yangtze River, in Yichang, China. The x-axis represents the radial velocity of target, which can be converted by Doppler frequency. The y-axis represents the detection range of radar. The target moving toward the radar produces positive velocity, while negative velocity means the target moves away from radar. A potential ship target around 200 m from the radar site is marked with an oval box in Fig. 1(a). Observe that the target echoes in the UHF radar do not behave like those from the traditional point targets in high frequency (HF) radar [21], which are seriously extended both in range dimension and Doppler (or velocity) dimension. In addition, the shape and size of the extension of the target echoes vary with the range and Doppler of the target. It indicates that the extended target (or area target) detection is involved in the UHF radar. Generally, the power of ship echoes is determined by the range and the radar cross section (RCS) of target, whereas the extension characteristics in the dimension of range and velocity are mainly related to the RCS and the velocity variations within the coherent integration time (CIT) of radar processing. However, for the UHF radar with high range resolution, the moving ship may walk multiple range cells within the CIT of radar, which causes the range extension. In the river channel, ship targets move at a constant speed along the riverbank. The radial velocity (i.e., the component along the direction of the radar) of the target changes rapidly as it approaches the radar, which causes the Doppler extension.

The echoes scattering from the water waves in the river are also involved in Fig. 1(a), as shown in the continuously distributed bright color area. The power of the river echoes is indicated in the right color bar. As a wide beam radar, the river echoes are severely broadened in the UHF radar, for example, the radial velocity below 2 m/s (i.e., marked by the black dotted lines) is completely covered by the river echoes. The strong signals at the 0 velocity are the echoes of static targets such as buildings and mountains. Both the river echoes and the building echoes are clutters for the ship target detection, which seriously degrade the radar detection performance. The target detection in the UHF radar is then divided into two regions: the clutter

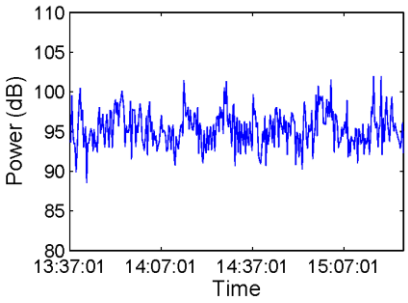

Fig. 2. The power variation of the river clutter at the 9th range bin.

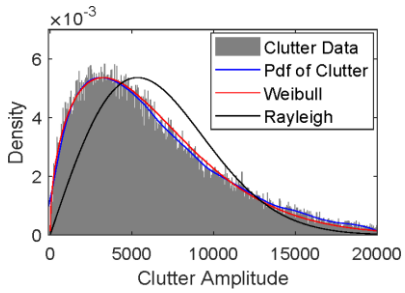

Fig. 3. Clutter distribution.

area (i.e., Region I) and the non-clutter area (i.e., Region II).

The Doppler spectrum at the 15th range bin (i.e., 225 m) is shown in the red curve in Fig. 1(b), in which the echo of the ship target is marked with an oval box. The cyan curve shows the Doppler spectrum at the same range one minute ago, and the blue curve shows the Doppler spectrum one minute later. Both the cyan and blue curve are free of ship echoes, i.e., only including the clutters. As shown in Fig. 1(b), the power of the ship is nearly 20 dB higher than that of the river clutter. However, the power of the target changes with time, whereas, the power of the clutters remains unchanged.

The fluctuation of the river clutter over a period of time is further analyzed. Fig. 2 shows the variation of the maximum power of river clutter at the 9th range bin in the R-D spectra from 13:37:01 pm to 15:26:31 pm, Oct 28th 2016. The statistical results show that the mean value of the power of the river clutter is 95.36 dB and the standard deviation is 2.33 dB, which is quite a small fluctuation. Similar statistical results can be observed at other range bins, which illustrates that the river clutter does not change drastically. Therefore, the clutter can be assumed to be wide-sense stationary over a period of time.

III. An Improved CA-CFAR Method

The amplitude distribution characteristics of the river clutter is analyzed and shown in Fig. 3. The gray part shows the statistical result of clutter amplitude, and the blue curve shows the corresponding probability density function (pdf). In addition, the fitting curves of the Rayleigh distribution (the black curve) and the Weibull distribution (the red curve) [22] are also shown. It indicates that the amplitude of the river clutter is closer to the Weibull distribution, i.e., the shape parameter is 1.4. The pdf of a Weibull distribution is given as

$$f(x)=\frac{b}{a}\left(\frac{x}{a}\right)^{b-1}e^{-(x/a)^b},\ x\geq 0 \qquad (1)$$

where a is the scale parameter and b is the shape parameter. The

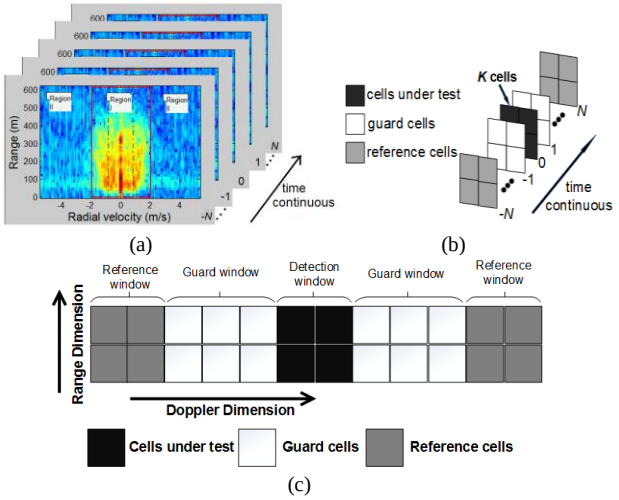

Fig. 4. Detection schematic. (a). R-D spectra stored in order. (b). 3D architecture of the improved method. (c). Detection schematic of the conventional method.

cumulative distribution function (cdf) is

$$F(x) = P(X \le x) = 1 - e^{-(x/a)^b}, x \ge 0 \tag{2}$$

Assuming we choose $2N+1$ R-D spectra stored in order, numbering $-N$, ..., -1, 0, 1, ..., N as shown in Fig. 4(a). Spectrum No.0 is the current one, in which a 2D sliding window with K cells under test (CUT) including both the range and Doppler cells is set as detection window. Another one-dimensional (1D) sliding window in time serials is set for the sequential spectra, leading to a 3D CFAR detection. Therein, No.1 and -1 are guard windows, and the rest are reference windows as shown in Fig. 4(b). Different from the traditional CA-CFAR method taken the surrounding units of CUT in a single spectrum as reference units (see in Fig. 4(c)), the improved method in Fig. 4(b) takes the cells of the leading and lagging R-D spectra as reference units to estimate the clutter power. This improved CA-CFAR method is more sensitive to the detection of the extended target in the strong river clutter, where the extension characteristics of the target echoes such as shape and size change rapidly in a short period of time.

The average clutter power X is computed as the sum of the clutter cells in the reference windows, that is

$$X = \sum_{i=1}^{M} x_i \tag{3}$$

where x represents clutter amplitude in a cell, M is the number of reference cells, therein,

$$M = K \cdot (2N - 2) \tag{4}$$

The clutter in these windows is identically independent distributed. The joint pdf of X is given by the product of the marginal pdfs.

$$f_M(x) = \prod_{i=1}^{M} f(x_i) = \left(\frac{b}{a}\right)^M e^{-\sum_{i=1}^{M}(\frac{x_i}{a})^b} \prod_{i=1}^{M}\left(\frac{x_i}{a}\right)^{b-1} \tag{5}$$

The calculation of (5) depends on the value of a and b, which is not known in closed form. [23] suggested a rational approximation of (5), that is

$$f_M(x) = \frac{cba^{-bM}}{\Gamma(M)}(cx)^{Mb-1}\exp\left[-\left(\frac{cx}{a}\right)^b\right] \tag{6}$$

where $\Gamma(\cdot)$ is the Gamma function, c can be identified as a scale parameter, which can be defined as

$$c = \frac{\Gamma(M + 1/b)}{M\Gamma(M)\Gamma(1+1/b)} \tag{7}$$

The first moment (the mean) of the distribution (6) is equal to the mean of the sum of the M Weibull distributed cells. Moreover, [24] analyzed the CA-CFAR processor in Weibull background based on the approximation formula (6) and confirmed its availability.

The false alarm probability P_{FA} can be calculated as [23]:

$$P_{FA} = \int_0^\infty P(CUT > TX) f_M(x) dx = \int_0^\infty e^{-(\frac{TX}{a})^b} f_M(x) dx \tag{8}$$

where T is the threshold product factor used in the CFAR detector. After some manipulations, we get

$$P_{FA} \cdot [1 + (T/c)^b]^M = 1 \tag{9}$$

Consequently, we can easily get

$$T = c(P_{FA}^{-\frac{1}{M}} - 1)^{\frac{1}{b}} \tag{10}$$

Obviously when b=1.4 as we obtained in Fig. 3, (7) is substituted in and (10) can be written as

$$T = \frac{\Gamma(M + 5/7)}{M\Gamma(M)\Gamma(12/7)}(P_{FA}^{-\frac{1}{M}} - 1)^{\frac{5}{7}} \tag{11}$$

As shown in (11), the threshold product factor T depends on the number of reference cells M and the false alarm probability P_{FA}.

IV. Experimental Results

The performance of the 3D CA-CFAR detector is tested using simulated area targets. The field experimental data without ship target echoes, measured in Yangtze River, are used as the clutter background. 100 area targets are totally simulated in the strong clutter region (i.e., Region I) of the R-D spectra. Herein, the radial velocities of these targets are between -2 and +2 m/s. The echoes of these area targets are extended by 3 to 6 cells in the range dimension and 6 to 14 cells in the Doppler dimension. In addition, the signal-to-clutter ratio (SCR) of these targets is adjustable to explore the relationship between detection probability (P_D) and SCR (i.e., SCR =10 dB, 14dB, or 18dB). The false alarm probability (P_{FA}) is also adjustable to explore the relationship between P_D and P_{FA} (i.e., P_{FA} is from 0.01 to 1). The parameter of CFAR is set as follows: N=2 and K=4 (i.e., 2 range cells and 2 Doppler cells). As shown in Fig. 4(b), 4 CUT, 8 guard cells and 8 reference cells are possessed in the 3D CFAR detector. For better comparison, the conventional 2D CA-CFAR method [13] is also conducted, in which 4 CUT (i.e., 2 range cells and 2 Doppler cells), 12 guard cells and 8 reference cells are processed as shown in Fig. 4(c).

Fig. 5 shows the simulated receiver operating characteristic (ROC) curves of detection probability (P_D) versus false alarm probability (P_{FA}) for varying SCR. These curves are not smooth because they are simulated random targets detection under the real clutter background. Nevertheless, the curves have clear trends and can still intuitively reflect the detection effect of different methods. Observe how P_D increases as SCR increases in both CA-CFAR methods for any given values of P_{FA}, as expected. Compared with the conventional CFAR method

This article has been accepted for publication in a future issue of this journal, but has not been fully edited. Content may change prior to final publication. Citation information: DOI 10.1109/LSP.2020.3015682, IEEE Signal Processing Letters

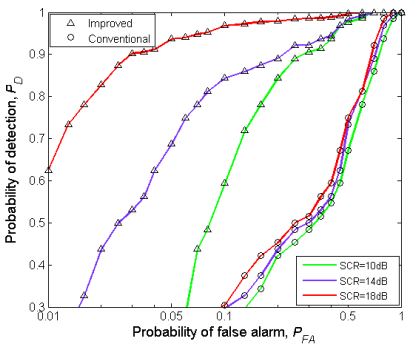

Fig. 5. ROC curves of P_D versus P_{FA} for varying SCR.

("○"), the detection probability of the improved method ("△") increases dramatically for a given SCR, e.g., P_D improves from 0.3 to more than 0.6 as P_{FA} = 0.1 for SCR=10dB. Moreover, the performance of conventional method can get a very limited promotion as SCR increases. On the contrary, the performance of improved method can get a prominent and visible promotion as SCR increases for a relatively low value of P_{FA}.

To further demonstrate the superiority of the improved CA-CFAR method, a field experiment of ship detection was conducted for the UHF radar in Yangtze River, Yichang, China. Fig. 6 shows some continuous time detection results under $P_{FA} = 1 \times 10^{-3}$ for both the two methods. Fig. 6(a) and (b) are the same R-D spectrum, so are Fig. 6(c) and (d) or Fig. 6(e) and (f). Fig. 6(a) (c) and (e) are detected with conventional CA-CFAR method, and Fig. 6(b) (d) and (f) are detected with improved CA-CFAR method. Moreover, the spectra of (a) (c) (e) are continuously collected in time with the interval time of 20.992s. These spectra show the movements of two potential ships: one moves away from radar site and finally disappears (in Region II); the other, marked with an oval box in (a) (c) (e), comes close to radar site at first, crosses the front of radar (i.e., in Fig. 6(c)) and then moves away (in Region I). Herein, detected target points have been marked out by black stars, and Region I has been marked out by black dotted lines.

As seen in Fig. 6(a), the target in strong clutter (i.e., in Region I) extends over multiple cells in both range and Doppler dimensions, but only a few points are detected by the conventional method. Whereas implementing the improved CA-CFAR method as shown in Fig. 6(b), much more target points are observed. What's more, there is no target point being detected in Region I in Fig. 6(c), which means false dismissal in this situation for the conventional CFAR. As a contrast, a lot of target points are still detected in Fig. 6(d) for the improved CFAR. In addition, the detection comparison between (e) and (f) ends up with exactly the same results. It shows that the improved CA-CFAR method can obtain a much higher P_D than the conventional method under the same conditions, which illustrates that the improved CA-CFAR method proposed in this paper has a better performance in target point detection in strong clutter. For the ship target detection in the clutter free background (i.e., in Region II), as shown in Fig. 6(a)-(d), both the conventional CFAR and the improved CFAR work well.

As the non-cooperative targets in Fig. 6, the number of targets and the state of motion are unknown. It is difficult to

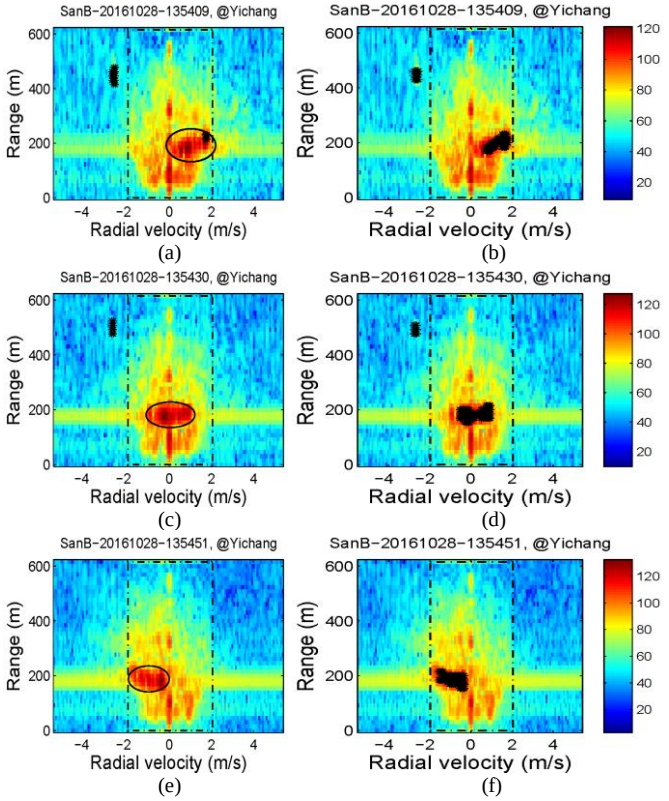

Fig. 6. Continuous time detection results of these two methods.
(a), (c), (e). Detected with conventional CA-CFAR method.
(b), (d), (f). Detected with improved CA-CFAR method.

distinguish between clutter and ship echoes in a single sample of the R-D spectrum, especially when ships are involved in the clutter. However, ship tracks rather than individual detections would identify the presence of the ship, based on the variables for measurements of range and radial speed [25]. As shown in Fig. 6(b), (d) and (f), the continuous time detection results reflect the trajectory of target moving in the clutter region, with changes of both range and radial velocity. From the detection results of Fig. 6(a) (c) and (e), due to the missed alarms, it is hard to recognize the trajectory of the target. It indicates that this improved CA-CFAR method has more stable and reliable detection performance, with potential application for ship tracking in the clutter background.

V. CONCLUSIONS

In this paper, a 3D CA-CFAR detector in range, Doppler and time serials of R-D spectra for detecting moving ship targets in strong clutter using UHF radar is proposed. Based on the time stationarity of river clutter, several leading and lagging R-D spectra collected in a continuous time were used to estimate the clutter power. The simulation results shows that compared with the conventional method, the P_D of the improved 3D CA-CFAR method improves by a factor of more than 2. The experimental data indicates that the proposed 3D CA-CFAR detects much more target points in strong river clutter when the conventional CFAR is almost ineffective. More ground truth data such as the automatic identification system (AIS) data are expected in the future experiment for a reasonable comparison.

REFERENCES

[1] F. Bandiera, D. Orlando, and G. Ricci, "CFAR detection of extended and multiple point-like targets without assignment of secondary data," *IEEE Signal Proc. Let.*, vol. 13, no. 4, pp. 240-243, Apr. 2006.

[2] H. Rohling, "Radar CFAR thresholding in clutter and multiple target situations," *IEEE Trans. Aerosp. Electron. Syst.*, vol. AES-19, no. 4, pp. 608–621, Jul. 1983.

[3] W. Liu, W. Xie, J. Liu, and Y. Wang, "Adaptive double subspace signal detection in Gaussian background—Part I: Homogeneous environments," *IEEE Trans. Signal Process.*, vol. 62, no. 9, pp. 2345-2357, 2014.

[4] M. Weiss, "Analysis of some modified cell-averaging CFAR processors in multiple-target situations," *IEEE Trans. Aerosp. Electron. Syst.*, vol. AES-18, no. 1, pp. 102-114, Jan. 1982.

[5] A. Abbadi, H. Bouhedjeur, A. Bellabas, T. Menni, and F. Soltani, "Generalized closed-form expressions for CFAR detection in heterogeneous environment," *IEEE Geosci. Remote Sens. Lett.*, vol. 15, no. 7, pp. 1011-1015, Jul. 2018.

[6] S. Blake, "OS-CFAR theory for multiple targets and nonuniform clutter," *IEEE Trans. Aerosp. Electron. Syst.*, vol. 24, no. 6, pp. 785-790, Nov. 1988.

[7] E. Conte, M. D. Bisceglie, and M. Lops, "Clutter-map CFAR detection for range-spread targets in non-Gaussian clutter. II. Performance assessment," *IEEE Trans. Aerosp. Electron. Syst.*, vol. 33, no. 2, pp. 444–455, Apr. 1997.

[8] J. R. Barnum, "Ship detection with high-resolution HF skywave radar," *IEEE J. Ocean. Eng.*, vol. OE-11, no. 2, pp. 196-209, Apr. 1986.

[9] H. J. Roarty, D. E. Barrick, J. T. Kohut, and S. M. Glenn, "Dual-use of compact HF radars for the detection of mid- and large-size vessels," *Turk. J. Elec. Eng. & Comp. Sci.*, vol. 18, no. 3, pp. 373-388, 2010.

[10] X. Huang, B. Wen, and F. Ding, "Ship detection and tracking using multi-frequency HFSWR," *IEICE Electron. Express*, vol. 7, no. 6, pp. 410-415, 2010.

[11] M. Kronauge and H. Rohling, "Fast two-dimensional CFAR procedure," *IEEE Trans. Aerosp. Electron. Syst.*, vol. 49, no. 3, pp. 1817-1823, 2013.

[12] J. Yan, X. Li, and Z. Shao, "Intelligent and fast two-dimensional CFAR procedure," in *2015 IEEE ICCP*, Guilin, China, Oct. 2015, pp. 461-463, DOI: 10.1109/ICCPS.2015.7454202.

[13] M. Zhang and X. Li, "An efficient real-time two-dimensional CA-CFAR hardware engine," in *2019 IEEE EDSSC*, June 2019, pp. 1-3, DOI: 10.1109/EDSSC.2019.8753926.

[14] A. Dzvonkovskaya, K.-W. Gurgel, H. Rohling, and T. Schlick, "HF radar WERA application for ship detection and tracking," *European Journal of Navigation*, vol. 7, no. 3, pp. 18-25, Dec. 2009.

[15] S. Maresca, J. Horstmann, R. Grasso, M. Coffin, K.-W. Gurgel, and T. Schlick, "Performance assessment of HF-radar ship detection," in *International Radar Symposium 2011*, Leipzig, Germany, Sept. 2011, pp. 131-136.

[16] Y. Lin, T. Lee, Y. Pan, and K. Lin, "Low-complexity high-resolution parameter estimation for automotive MIMO radars," *IEEE Access*, vol. 8, pp. 16127-16138, 2020, DOI: 10.1109/ACCESS.2019.2926413.

[17] Y. D. Hou, B. Y. Wen, and Y. H. Yang *et al.*, "Two-dimensional river flow patterns observed with a pair of UHF radar system," *Int. J. Antennas Propag.*, pp. 1-11, Apr. 2017. DOI: 10.1155/2017/4792324.

[18] Y. Yang, B. Wen, C. Wang, and Y. Hou, "Two-dimensional velocity distribution modeling for natural river based on UHF radar surface current," *J. Hydrol.*, vol. 577, Oct. 2019. DOI: 10.1016/j.jhydrol.2019.123930.

[19] C. Randell, D. Power, and R. Khan, "Ocean clutter characteristics for a coherent Doppler UHF radar," in *Oceans Conference Record (IEEE) (Cat. No.00CH37158)*, Providence, RI, USA, 2000, pp. 1515-1520, vol. 3.

[20] D. D. Crombie, "Doppler spectrum of sea echo at 13.56 Mc./s," *Nature*, vol. 175, no. 4459, pp. 681-682, 1955.

[21] B. Lu, B. Wen, Y. Tian, and R. Wang, "A vessel detection method using compact-array HF radar," *IEEE Geosci. Remote Sens. Lett.*, vol. 14, no. 11, pp. 2017-2021, 2017.

[22] F. D. Almeida Garc á, A. C. Flores Rodriguez, G. Fraidenraich, and J. C. S. Santos Filho, "CA-CFAR detection performance in homogeneous Weibull clutter," *IEEE Geosci. Remote Sens. Lett.*, vol. 16, no. 6, pp. 887-891, Jun. 2019.

[23] Y. Dong, Distribution of X-band high resolution and high grazing angle sea clutter, *Defense Science and Technology Organisation (DSTO)*, Edinburgh, South Australia, Jul. 2006.

[24] K. Siddiq and M. Irshad, "Analysis of the cell averaging CFAR in Weibull background using a distribution approximation," in *IEEE-IC4 2009*, Karachi, Pakistan, 2009, pp. 1-5.

[25] J. F. Vesecky and K. E. Laws, "Identifying ship echoes in CODAR HF radar data: A Kalman filtering approach," in *OCEANS 2010*, Sept. 2010, pp. 1-8.